Tight-binding model for carbon from the third-generation LMTO method: A study of transferability

D NGUYEN-MANH*, T SAHA-DASGUPTA[†,‡] and O K ANDERSEN[†]

Department of Materials, University of Oxford, Parks Road, Oxford OX1 3PH, UK
[†]Max-Planck-Institut für Festkorperforschung, 70569 Stuttgart, Germany
[‡]Also at S.N. Bose National Centre for Basic Science, Bidhan Nagar, Kolkata 700 098, India

Abstract. The third-generation LMTO method provides a new wave function basis set in which the energy dependence of the interstitial region and inside muffin–tin (MT) spheres is treated on an equal footing. Within the improved method, basis functions in the interstitial are the screened spherical waves (SSWs) with boundary condition defined in terms of a set of 'hard' sphere radii a_{RL}. Energy eigenvalues obtained from the single-particle Schrödinger equation for MT potential is energetically accurate and very useful for predicting a reliable first-principles tight-binding (TB) model of widely different systems. In this study, we investigate a possibility of the new basis sets transferability to different environment which could be crucial for TB applications to very large and complicated systems in realistic materials modelling. For the case of C where the issue of sp^2 vs sp^3 bonding description is primarily important, we have found that by downfolding the unwanted channels in the basis, the TB electronic structure calculations in both hexagonal graphite and diamond structures are well compared with those obtained from the full LDA schemes if we use the same choice of hard sphere radii, a_{RL} and a fixed, arbitrary energy, ϵ_ν. Moreover, the choice is robust and transferable to various situations, from different forms of graphite to a wide range of coordination. Using the obtained minimal basis set, we have been investigating the TB Hamiltonian and overlap matrices for different structure types for carbon, in particular we have predicted the on-site and hopping parameters (γ_1, γ_2, ..., γ_6) within an orthogonal representation for Slonczewski–Weiss–McClure (SWMcC) model of the Bernal structure. Our theoretical values are in excellent agreement with experimental ones from magnetoreflection measurements of Fermi surfaces for hexagonal graphite.

Keywords. Carbon materials; electronic structure; *ab initio* calculations; tight-binding; transferability.

1. Introduction

The past decade has witnessed an explosion in number of applications of the tight-binding (TB) model to simulating the structural and cohesive properties of materials (Turchi *et al* 1998). This is due to the TB model being the simplest scheme that includes correctly the underlying quantum mechanical character of covalent bond in variety of materials including semiconductors, transition metals and even more complex materials with mixed metallic/ionic and covalent bonding. The conventional semiempirical TB method, however, suffers from uncertainty of how best to choose the TB parameters that enter the scheme. Therefore, it is desirable to develop a direct and deterministic way of computing the TB parameters out of first-principles calculations.

The linear muffin–tin orbital (LMTO) method of the first and second generations implemented in the basis of the screened and energy-independent muffin–tin (MT) orbitals (Andersen and Jepsen 1984; Andersen *et al* 1985) has already been proved to be a powerful method

for providing first-principles parameters. Nevertheless, it lacks the desirable flexibility to be used as an automatic scheme for providing simple and tight-binding basis sets for a broad class of materials. In this paper we shall be using an improved version of the LMTO method viz. the third generation LMTO method (Andersen *et al* 1998) which precisely satisfies this objective. We shall demonstrate this by deriving tight-binding electronic structure calculations within different local environment for C including graphite and diamond structures with sp^2 and sp^3 bonding, respectively.

Carbon science has been revolutionized by the discovery and synthesis of fullerenes (Kroto *et al* 1985) and subsequent identification of nanotubes (Iijima 1991). On the other hand, the outstanding chemical and physical properties of tetrahedral amorphous carbon (Mckenzie 1996) are again the subject of interest with the discovery of so-called medium-range order at nanoscale measured by fluctuation electron microscopy (Chen *et al* 2001). The origin of medium-range order in *a*-C is still mysterious and computational simulation with an accurate tight-binding based interatomic potential at very large scale, which is beyond the present state-of-art of Car–Parrinello scheme, could help to gain more understanding of its

---

*Author for correspondence

structure. The long-term purpose of this project is to study the extraction of transferable tight-binding parameters from third-generation LMTO to be fed into the new bond-order potentials scheme (Nguyen-Manh *et al* 2000).

2. Third-generation LMTO formalism

The crucial difference between the traditional and the improved LMTO method lies in the description of interstitial region between MT spheres surrounding around the position of atoms. In the new version, the energy dependence of the interstitial is treated on an equal footing with the MT spheres, so that the single-particle energies obtained from the Hamiltonian and overlap matrices in the new basis set is energetically more accurate. Within 3rd generation LMTO, the basis functions in the interstitial are the screened spherical waves (SSWs) which are the solutions of the wave equation (Andersen *et al* 1998)

$$[\Delta + \boldsymbol{e}]\boldsymbol{y}(\boldsymbol{e}, r) = 0, \tag{1}$$

with boundary conditions defined for a structure with sites R. The boundary condition is defined in terms of a set of hard sphere radii, a_{RL} ($L \equiv 1\,m$) being concentric with each MT sphere centred at R such that when $\boldsymbol{y}_{RL}^{a}(\boldsymbol{e}, r_R)$ is expanded in spherical harmonics, $Y_{R',L'}(\hat{r}_{R'})$ about its neighbouring sites R', then each component either vanishes at a radius, $r_{R'} = a_{R'L'}$, or is a regular solution at that site. The hard sphere radii, for different L channels, are considered to be different while a_{RL} for channels with high-l values are taken to be zero, so that the radial parts of the high-l projection become spherical Bessel functions $j_l(\boldsymbol{k}_R)$ with $\boldsymbol{k}^2 = \boldsymbol{e}$. For the low-l components, the range of SSWs depend on the choice of hard sphere, a_{RL} and the energy.

The radial derivatives of the SSWs at the hard spheres are defined, within the screened $\{a\}$ representation, by the dimensionless slope matrix, $S_{R'L',RL}^{a}(\boldsymbol{e})$ which in turn can be expressed in terms of the conventional KKR structure constant. In order to solve the Schrödinger equation, one defines the kinked partial wave (KPW)

$$\Phi_{RL}^{a}(\boldsymbol{e}, r_R) = [\boldsymbol{f}_{Rl}^{a}(\boldsymbol{e}, r_R) - \boldsymbol{j}_{Rl}^{a}(\boldsymbol{e}, r_R)]Y_L(\hat{r}_R) + \boldsymbol{y}_{Rl}^{a}(\boldsymbol{e}, r_R), \tag{2}$$

where $\boldsymbol{f}_{Rl}^{a}(\boldsymbol{e}, r_R)$ and $\boldsymbol{j}_{Rl}^{a}(\boldsymbol{e}, r_R)$ are the radial partial wave for each strong scattering channel outwards from the origin to the MT radius, s_R and inwards in zero potential from s_R to the hard-sphere radius, a_{RL}, respectively. This KPW is everywhere continuous, but has kinks of size $[S_{R'L',RL}^{a}(\boldsymbol{e}) - D\{\boldsymbol{j}_{RL}(\boldsymbol{e}, a_{RL})\} \boldsymbol{d}_{R'L',RL}]$, as shown in figure 1, where $D(f(x)) = \partial\ln|f(x)|/\partial\ln x$ denotes the radial logarithmic derivative. Like the slope matrix, the kink matrix is not Hermitian but the matrix
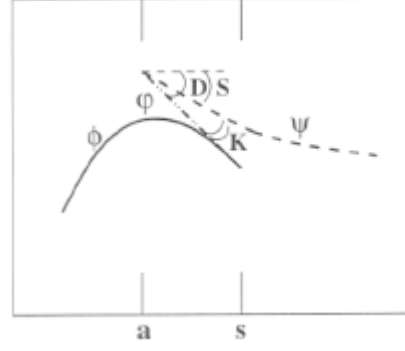
Figure 1. Various components of kinked partial wave within the third generation LMTO scheme.

$$K_{R'L',RL}^{a}(\boldsymbol{e}) \equiv a_{R'L'}[S_{R'L',RL}^{a}(\boldsymbol{e}) - D\{\boldsymbol{j}_{RL}(\boldsymbol{e}, a_{RL})\}\boldsymbol{d}_{R'L',RL}], \tag{3}$$

is. It is shown from Andersen *et al* (1998) that the screened KKR matrix, $K^{a}(\boldsymbol{e}_n)$ at a fixed arbitrary energy, $\boldsymbol{e}_n$ is the negative of the Hamiltonian and its first energy derivative, $\dot{K}^{a}(\boldsymbol{e}_n)$ is the overlap matrix in the basis of KPW. Solving the KKR equations lead to exact solution of the Schrödinger equation, but it is more practical to solve the set of eigenvalue equations involving Hamiltonian, H and overlap, O matrices as is done in the LMTO method. The energy-independent set of improved LMTO, $|\boldsymbol{c}\rangle = |\Phi\rangle - |\dot{\Phi}\rangle\dot{K}^{-1}K$ is complete to linear order with respect to the MT Hamiltonian and yields single-particle energies, $\boldsymbol{e}_n$ with errors proportional to $(\boldsymbol{e} - \boldsymbol{e}_n)^4$. For comparison, previous generation LMTO set has single-particle energy errors of order $(\boldsymbol{e} - \boldsymbol{e}_n)^2$. Additional feature of the third-generation LMTO method is that it enables us to make the *m*-dependent downfolding which is very important for deriving the few-orbitals TB Hamiltonians.

Renormalizing and subsequently, Lowdin orthonormalizing the KPWs, $|\overline{\Phi}\rangle$, lead to a formalism analogous to conventional one with h, o, p now redefined as

$$h = -\tilde{\dot{K}}^{-1/2}\tilde{K}\tilde{\dot{K}}^{-1/2},$$
$$o = -\ddot{h}/2, \quad p^2 + o = -\dddot{h}/6, \tag{4}$$

where $\tilde{\dot{K}} = \langle\tilde{f}|\tilde{f}\rangle$ is the overlap matrix for the renormalized KPWs. As a result, ones recover the conventional expressions for the MT-Hamiltonian in the completely orthogonal representation as a power series in two-centred Hamiltonian, h:

$$\langle\boldsymbol{c}^{\text{ort}}|H_{\text{mt}} - \boldsymbol{e}_n|\boldsymbol{c}^{\text{ort}}\rangle = h - hoh + h[oho - \tfrac{1}{2}(ph + hp)]h + \cdots \tag{5}$$

where

$$|\boldsymbol{c}^{\text{orth}}\rangle \equiv |\overline{c}\rangle\langle\overline{c}|\overline{c}\rangle^{-1/2} \sim |\overline{c}\rangle(1 + oh)^{-1}$$
$$= |\boldsymbol{c}^{g}\rangle \text{ with } |\vec{=}\rangle = |\overline{\overline{O}}\rangle + |\dot{\overline{O}}\rangle h.$$

3. Orthogonal TB model for graphite

3.1 *Band structure calculations*

Natural graphite occurs in two crystal structures: the Bernal or hexagonal ($P6_3/mmc$) and the rhombohedral ($R\bar{3}m$) structures. In difference to simple graphite structure ($P6/mmm$) which has an AAA-stacking with all carbon atoms in consecutive layers located on top of each other, the Bernal structure possesses an ABAB-stacking while rhombohedral graphite has an ABC-stacking. At zero Kelvin, the distance between nearest-neighbours is 1·42 Å and the interlayer separations calculated by minimizing total energy obtained by first-principles calculations are 3·335 Å, 3·35 Å and 3·34 Å for simple, hexagonal and rhombohedral graphite, respectively. The converged LDA band structure for hexagonal graphite is shown in figure 2 where the zero of energy is the Fermi level. In order to highlight the role of different orbital-projected contributions, we have used 'flat' band structure representation (Neumann *et al* 1998) for 2s, $2p_x + 2p_y$ (in the graphitic plane) and $2p_z$ (perpendicular to the graphitic plane). The strong bonding within the layers is described by sp^2 hybridized 2s, $2p_x$ and $2p_y$ atomic orbitals (**s** states) and the weak interlayer bonding is derived from the overlap between $2p_z$ orbitals (**p** states).

We have applied the improved formalism of 3rd-generation LMTO method presented in §2 for generating TB Hamiltonian for graphite using C-sp^3 basis set (all empty spheres *spd* and C-*d* channels are downfolded). The TB calculations have been performed within the orthogonal representation for Hamiltonian from (5). The hard sphere radii, a_s and a_p for 2s and 2p orbitals respectively, and also the fixed linearized energy, e_n have been optimized in order to get the correct electronic structure for all the valence band states and the two first conduction band states along the K–H direction of the Brillouin zone where a zero-gap semiconductor or semimetal behaviour is observed. For hexagonal graphite, we have found that $a_s = 1·54$ a.u., $a_p = 1·33$ a.u. and $e_n = -0·77$ Ry. In figure 3 we compare the LDA band structure (full lines) with results obtained from the Hamiltonian matrix truncated to

1st, 2nd, 3rd, 4th, 5th and 10th nearest neighbour (NN) (dashed line), respectively. We can see clearly that when 4th NN interlayer interactions are included into consideration, the degeneracy along G–A line is lifted and it is possible to get an accurate description of valence band structure within the orthogonal TB formalism after 10th NN calculations.

3.2 *SWMcC-model parameters of the **p** band bonding*

As the present TB formalism is free from fitting parameters and purely deterministic, it is interesting to deduce from calculated band structures the well known seven SWMcC interaction parameters for the hexagonal graphite (Slonczewski and Weiss 1955, 1958; McClure 1957). These parameters are determined within an orthogonal TB representation using the atomic **p** orbitals as shown in figure 4. While the parameter, **g**, represents the interaction between neighbouring atoms in a graphitic monolayer, the parameters **g** ($i = 1$–5) represent different interactions between two neighbouring or next-neighbouring graphitic planes. The **g** $= \Delta$ parameter is the chemical-shift between A and B atoms. The SWMcC model extends the linear dispersion law of the graphic monolayer to the 3D case. This model is valid in some regions of the Brillouin zone, such as the neighbouring of the six vertical edges H–K–H. Along a vertical axis (H–K–H or H′–K′–H′), the eigenvalues of Hamiltonian are given by

$$\varepsilon_1^0 = \Delta + \mathbf{g}\Gamma + \frac{1}{2}\mathbf{g}\Gamma^2, \tag{6}$$

$$\varepsilon_2^0 = \Delta - \mathbf{g}\Gamma + \frac{1}{2}\mathbf{g}\Gamma^2, \tag{7}$$

$$\varepsilon_3^0 = \frac{1}{2}\mathbf{g}\Gamma^2, \tag{8}$$

where $\Gamma = 2\cos(k_z c_0/2)$ and the wave vector, k_z is measured from the K point. At the edge H–K–H of the Brillouin zone, in the plane A–H, the eigenvalues are given by
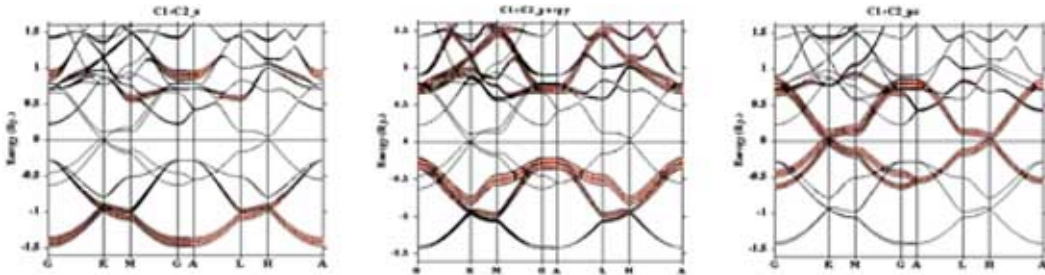
Figure 2. LDA orbital-projected bands for hexagonal graphite.
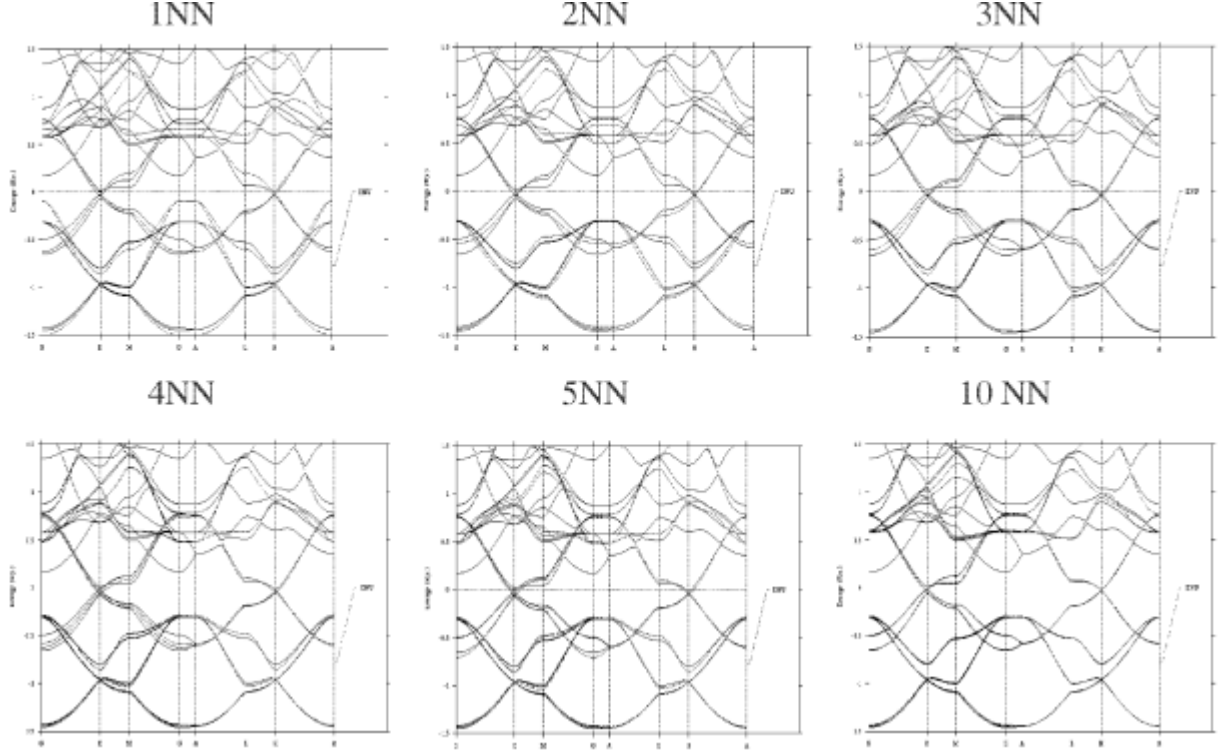
Figure 3. Third generation LMTO band structure calculations for 1NN, 2NN, 3NN, 4NN, 5NN and 10NN (solid line) compared with the LDA energy bands (dashed line) for hexagonal graphite.
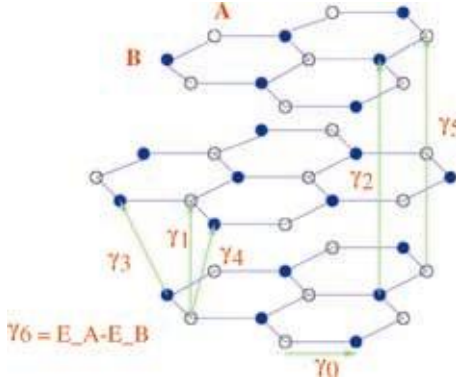
Figure 4. The SWMcC TB parameters between individual atoms in the graphite lattice.

Table 1. Values of the SWMcC-model parameters (in eV) for hexagonal graphite from the present work in comparison with the plane-wave pseudopotential calculations and with a collection of the best experimental evaluations (Charlier and Michenaud).

Parameter	Present work	Plane-wave method	Experimental
g	3·142	2·598	3·16 ± 0·05
g	0·411	0·364	0·39 ± 0·01
g	− 0·018	− 0·014	− 0·02 ± 0·002
g	0·310	0·319	0·315 ± 0·015
g	0·042	0·177	0·044 ± 0·024
g	0·043	0·036	0·038 ± 0·005
g	− 0·015	− 0·026	− 0·008 ± 0·002

$$\frac{d\boldsymbol{e}}{d(k')^2}\Big|_{\boldsymbol{e}=\boldsymbol{e}_1^0,\,k=0} = -\left(\frac{2\boldsymbol{p}}{\sqrt{3}}\right)^2 \frac{\boldsymbol{g}_0^2}{\boldsymbol{e}_3-\boldsymbol{e}_1^0}(1-\boldsymbol{m})^2, \qquad (9)$$

$$\frac{d\boldsymbol{e}}{d(k')^2}\Big|_{\boldsymbol{e}=\boldsymbol{e}_2^0,\,k=0} = -\left(\frac{2\boldsymbol{p}}{\sqrt{3}}\right)^2 \frac{\boldsymbol{g}_0^2}{\boldsymbol{e}_3-\boldsymbol{e}_2^0}(1+\boldsymbol{m})^2, \qquad (10)$$

$$\frac{d\boldsymbol{e}}{dk'}\Big|_{\boldsymbol{e}=\boldsymbol{e}_3^0,\,k=0} = \pm\frac{2\boldsymbol{p}}{\sqrt{3}}\boldsymbol{g}\Gamma, \qquad (11)$$

where $\boldsymbol{m}= 2(\boldsymbol{g}/\boldsymbol{g})\cos(k_z c_0/2)$. Table 1 presents a set of calculated values of the SWMcC parameters from 3rd-generation LMTO method and compares it with the theoretical plane-wave *ab initio* method and experimental data from different measurements of the Fermi surface (Charlier and Michenaud 1992). Our values are in excellent agreement with experimental data.

4. Transferable parameters for carbon

As it has been emphasized in §2, the new basis set of 3rd generation LMTO scheme is more accurate due to the

introduction of a set of hard sphere radii, a_{RL}. In this section, we use the values of $a_s = 1\cdot54$ a.u., $a_p = 1\cdot33$ a.u. and the fixed energy of $\mathbf{e}_{nu} = -0\cdot77$ Ry which is considered as centre of valence band as the three main parameters for calculating electronic energy bands of different crystalline structures.

4.1 *Transferability between graphite and diamond*

Study of the electronic band structure for graphite and diamond-like carbon plays a crucial role in understanding the relationship between sp^2 and sp^3 bonding. On the other hand, there is a well known transformation path from rhombohedral graphite to diamond which minimizes the energy at each value of the bond length bet-

ween layers (Fahy *et al* 1986). We allow the Hamiltonian matrix to extend to 12th NN distance of the diamond structure as it is found from previous investigation for Si that with sp^3 basis set it is certain to obtain an accurate first-principles band structure from the present TB scheme (Saha Dasgupta *et al* 2000). Figure 5 shows a comparison of band structure of hexagonal graphite, diamond and rhombohedral graphite calculated with the above fixed parameters. For the diamond structure, we use the lattice parameter $a = 6\cdot6754$ a.u. which has been found from first-principles calculations within FLAPW method (Nguyen-Manh *et al* 2001). The real-space cluster corresponding to 12th NN distance for diamond-like carbon has the radius, R_c of 11·5625 a.u. The figure demonstrates a remarkable agreement between the TB and the
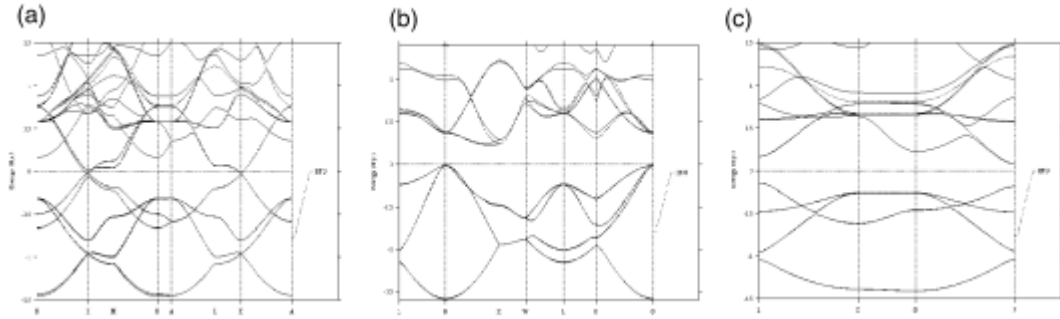
Figure 5. Third generation LMTO energy bands calculated with $a_s = 1\cdot54$ a.u., $a_p = 1\cdot33$ a.u., $E_n = 0\cdot77$ a.u. and $R_c = 11\cdot5625$ a.u. for hexagonal graphite (**a**), diamond (**b**) and rhombohedral graphite (**c**) (solid line) and compared with the corresponding LDA calculations (dashed line).
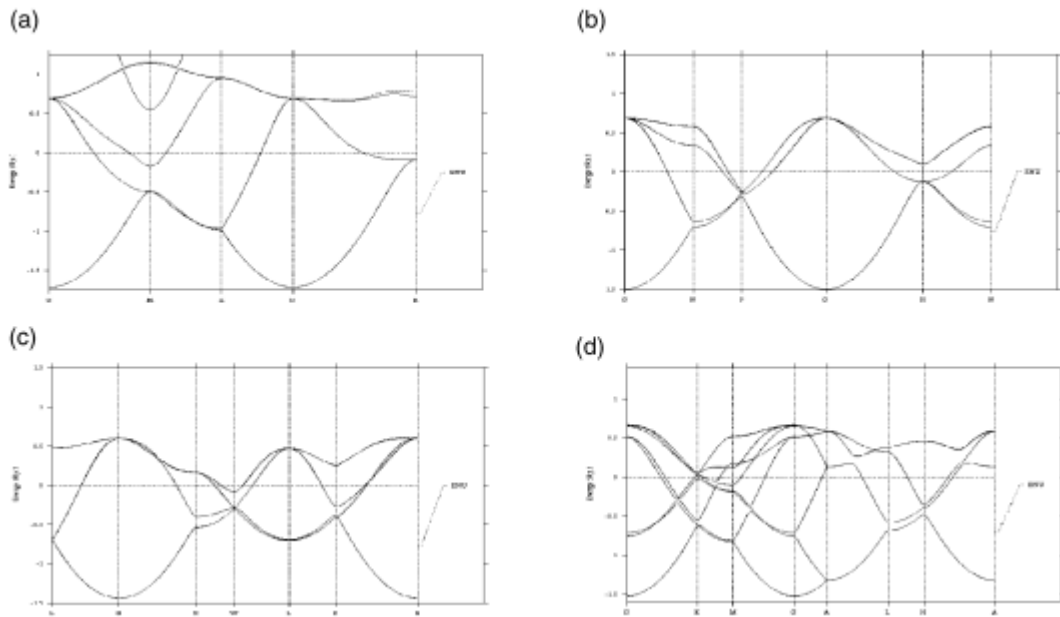
Figure 6. The same as in figure 5 for simple cubic (**a**), *bcc* (**b**), *fcc* (**c**) and *hcp* (**d**) structures.

LDA calculations not only for description of all valence bands but also for lowest conduction band in three considered structures.

4.2 *Transferability to higher coordination numbers*

It is very important for transferability of TB scheme that its environmental dependence of two-centre Hamiltonian matrix can be extended to describe properly the higher-coordinated (metallic) structures in addition to the graphite and diamond structures (Tang *et al* 1996; Nguyen-Manh *et al* 2000). We use the diamond structure as the reference structure for carbon with the four parameters: a_s, a_p, E_ν and R_c. Figure 6 shows the electronic band structure calculation for simple cubic ($a = 3.2810$ a.u.), *bcc* ($a = 4.4058$ a.u.), *fcc* ($a = 5.7074$ a.u.) and *hcp* ($a = 3.9251$, $c = 6.4097$ a.u.) with all lattice parameters obtained from the FLAPW results (Nguyen-Manh *et al* 2001). In figure 6, the TB calculation reproduces very well almost all the metallic bands within the present sp^3 basis set.

5. Conclusions

We have employed the third generation LMTO method to study various tight-binding electronic energy bands of carbon in different structure types. For the ground-state hexagonal graphite structure we have calculated, within the SWMcC model for the p bands, six TB parameters which are in excellent agreement with experimental measurements of Fermi surface. By using the orthogonal representation, we have shown that the hard-sphere radii, a_s and a_p, and the fixed linearized energy, E_ν, are the important parameters to reproduce the correct electronic energies not only for graphite and diamond-like carbon but also for higher-coordinated metallic structures. This preliminary study being free from any fitting procedure, provides a powerful base for investigating the transferability of TB Hamiltonian (and overlap) matrices within the third generation LMTO or more accurate NMTO (Andersen *et al* 2000) schemes.

References

Andersen O K and Jepsen O 1984 *Phys. Rev. Lett.* **53** 2571
Andersen O K, Jepsen O and Glotzel D 1985 in *Highlights of condensed matter theory* (eds) F Bassani *et al* (Amsterdam: North-Holland) p. 59
Andersen O K, Arcangeli C, Tank R W, Saha-Dasgupta T, Krier G, Jepsen O and Dasgupta I 1998 in *Tight-binding approach to computational materials science*, *MRS Proceedings* (eds) P E A Turchi *et al* (Warrendale: Materials Research Society) **491** p. 3
Andersen O K, Saha-Dasgupta T, Tank R W, Arcangeli C, Jepsen O and Krier G 2000 in *Electronic structure and physical properties of solids* (ed.) H Dreysse (Lecture Notes in Physics, Springer) p. 3
Charlier J C and Michenaud J P 1992 *Phys. Rev.* **B46** 4531
Chen X, Gibson J M, Sullivan J, Friedmann T and Voyles P 2001 *MRS Proceedings* (Warrendale: Materials Research Society) to be published
Fahy S, Louie S G and Cohen M 1986 *Phys. Rev.* **B34** 1191
Kroto H W *et al* 1985 *Nature* (*London*) **318** 162
Iijima S 1991 *Nature* (*London*) **356** 354
McClure J W 1957 *Phys. Rev.* **108** 612
Mckenzie D R 1996 *Rep. Prog. Phys.* **59** 3611
Neumann A, Nguyen-Manh D, Kjekshus A and Sutton A 1998 *Phys. Rev.* **B57** 11149
Nguyen-Manh D, Pettifor D G and Vitek V 2000 *Phys. Rev. Lett.* **85** 4136
Nguyen-Manh D *et al*, to be published
Saha Dasgupta T *et al*, to be published
Slonczewski J C and Weiss P R 1955 *Phys. Rev.* **99** 636
Slonczewski J C and Weiss P R 1958 *Phys. Rev.* **109** 272
Tang M S, Wang C Z, Chan C T and Ho K M 1996 *Phys. Rev.* **B53** 979
Turchi P E A, Gonis A and Colombo L (eds) 1998 in *Tight-binding approach to computational materials science*, *MRS proceedings* (Warrendale: Materials Research Society)